Earth and Planetary Science Letters 563 (2021) 116878

Contents lists available at ScienceDirect

Earth and Planetary Science Letters

www.elsevier.com/locate/epsl

Along-strike variations in intermediate-depth seismicity and arc magmatism along the Alaska Peninsula

S. Shawn Wei [a,*], Philipp Ruprecht [b], Sydney L. Gable [a], Ellyn G. Huggins [b], Natalia Ruppert [c], Lei Gao [d], Haijiang Zhang [d]

[a] Department of Earth and Environmental Sciences, Michigan State University, East Lansing, MI, USA
[b] Department of Geological Sciences and Engineering, University of Nevada, Reno, NV, USA
[c] Alaska Earthquake Center, University of Alaska Fairbanks, Fairbanks, AK, USA
[d] School of Earth and Space Sciences, University of Science and Technology of China, Hefei, Anhui, China

ARTICLE INFO

Article history:
Received 30 September 2020
Received in revised form 8 February 2021
Accepted 5 March 2021
Available online xxxx
Editor: R. Bendick

Keywords:
subduction zone
Alaska Peninsula
intermediate-depth earthquakes
arc magmatism

ABSTRACT

The Alaska Peninsula section of the Aleutian-Alaska subduction zone exhibits significant along-strike variations in plate coupling, earthquakes, and arc magmatism. Here we use regional and teleseismic data from 1990 to 2018 to investigate intermediate-depth intra-plate seismicity beneath the Alaska Peninsula. The distribution of these events shows five distinct segments from southwest to northeast: Unimak, Pavlof, Shumagin, Semidi, and Kodiak. We identify two double seismic zones (DSZs) in the Pavlof and Semidi segments but not in others. The magnitude-frequency relationship of these earthquakes (*b*-value) also varies along strike, suggesting more fluids in the southwestern segments and closer to the slab top interface. We also evaluate trace elements of arc lavas in the Alaska Peninsula. Th/La ratios indicate a significant amount of sediments subducted in the Semidi segment that includes Aniakchak and Veniaminof, and the sediment signature peaks beneath the Black Peak volcano. In contrast, high Pb/Th but low Th/La ratios from southwestern volcanoes suggest high fluids released from the subducted slab. In sum, our observations suggest that the slab is more hydrated and thus undergoing more intensive dehydration in the southwest than in the northeast, whereas more sediments are subducted in the northeast than in the southwest. These along-arc changes are generally in agreement with previous studies of plate coupling and the crustal structure of the incoming plate. Moreover, the complexities beyond the monotonic changes imply that the intermediate-depth intra-plate seismicity and sub-arc melting are influenced by not only the pre-existing fabrics in the incoming plate, but also the subducted sediments and plate stress state.

1. Introduction

Subduction zones drive material exchange between the Earth's surface and its interior. Near the oceanic trench, a subducting plate is hydrated along the plate-bending faults in the form of hydrous minerals (Shillington et al., 2015). Water and marine sediments enter the trench as part of the subducting plate and return through flux melting via arc magmatism (van Keken et al., 2011; Grove et al., 2012). A series of dehydration reactions of hydrous minerals occur under a variety of pressure-temperature conditions in the subducted slab. For instance, the breakdowns of lawsonite in the crust and antigorite in the mantle release a large volume of water (Guiraud et al., 2001; Hacker et al., 2003). During the *in-situ* dehydration reactions or the migration of the released fluids from the source (Faccenda et al., 2012), the increased pore fluid pressure can reduce the effective pressure to trigger intermediate-depth intra-plate earthquakes. This mechanism is referred to as dehydration embrittlement (Kirby et al., 1996) or more generalized fluid-related embrittlement (Wei et al., 2017). Therefore, the distribution of intermediate-depth earthquakes at 50–300 km depths is potentially indicative of free fluids in a slab that most likely come from dehydration reactions (e.g., Hacker et al., 2003; Yamasaki and Seno, 2003).

More intriguingly, a double seismic zone (DSZ), in which intermediate-depth earthquakes occur along two layers parallel to the dip of the subducting slab, is observed in several subduction zones (e.g., Yamasaki and Seno, 2003; Brudzinski et al., 2007). The upper plane is usually confined in the slab crust and uppermost mantle with downdip compressional stresses, whereas the lower plane is about 20–40 km deep from the slab surface with downdip

* Corresponding author.
E-mail address: swei@msu.edu (S.S. Wei).

https://doi.org/10.1016/j.epsl.2021.116878
0012-821X/

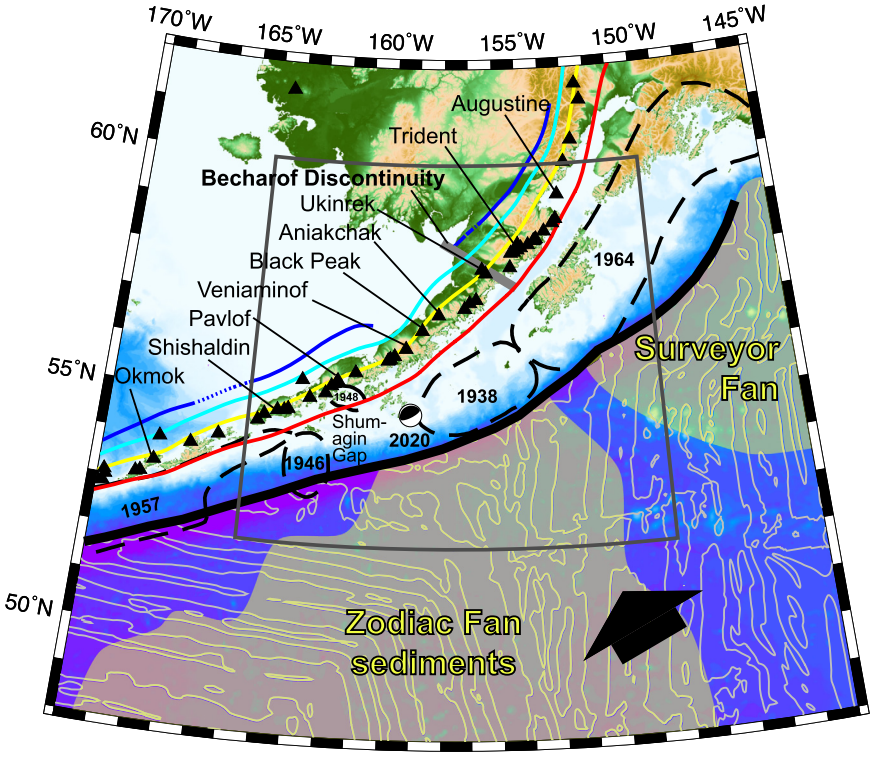

Fig. 1. Tectonic map of the Alaska Peninsula and adjacent regions. The bold black arrow indicates that the Pacific Plate subducts along the Alaska trench. Black triangles indicate Holocene volcanoes. Black dashed contours outline the rupture zones of previous megathrust earthquakes (Davies et al., 1981). The beachball indicates the M7.8 Simeonof earthquake on July 22, 2020. Red, yellow, cyan, and blue curves show the Alaska slab surface at 50, 100, 150, and 200 km depths, respectively, based on the Slab2 model (Hayes et al., 2018). Gray contours on the Pacific Plate outline the seafloor magnetic anomalies (Maus et al., 2009). Yellow shaded areas show the significant sediment input to the Alaska Trench (von Huene et al., 2012). The dark gray box indicates the study region in this paper. (For interpretation of the colors in the figure(s), the reader is referred to the web version of this article.)

tensional events. These phenomena are generally explained by a combination of slab unbending and fluid-related embrittlement (e.g., Wang, 2002; Hacker et al., 2003). The existence of a DSZ thus may serve as indirect evidence of fluids or volatiles in the slab mantle >20 km beneath the slab Moho. Although a DSZ has been observed in many, if not all, subduction zones (Brudzinski et al., 2007; Florez and Prieto, 2019), a study in NE Japan with a higher spatial resolution shows a sporadic rather than continuous lower plane (Igarashi et al., 2001), suggesting that deeper parts of the slab mantle are not uniformly hydrated.

Geochemical tracers have been developed to track fluids and melts within convergent margins (Hawkesworth et al., 1997; Plank and Langmuir, 1998; Kelemen et al., 2003; Grove et al., 2012). Besides the first-order factors like plate age and geometry that control dehydration and melting (van Keken et al., 2011), these processes may be also a function of the thickness and degree of hydration of the downgoing plate as well as the type of subducting sediment (Singer et al., 2007; Plank, 2014). Collectively, these parameters control the magma genesis in arcs prior to any interaction with and residence within the overriding crust (Hildreth and Moorbath, 1988; Winslow et al., 2020).

The Aleutian arc is an excellent endmember among convergent margins to deconvolve the various components that may contribute to arc magmatism (e.g., Miller et al., 1994; Class et al., 2000; Kelemen et al., 2003; Plank, 2005; Singer et al., 2007; Yogodzinski et al., 2015). Slab recycling has been reconciled mostly in segments of the Aleutians using trace element and isotope signatures, which include melts of the subducting sediment (e.g., Plank, 2005), the altered oceanic crust (AOC) (e.g., Kelemen et al., 2003) and hydrothermal contributions (e.g., Miller et al., 1994). How magma generation continues to the east along the Alaska Peninsula has yet to be constrained. The exceptionally distinct along-strike variations in sediment input offshore the Alaska Peninsula allow us to test specifically whether such changes pass through the subduction system and get imparted onto the arc source magmas. In combination with geophysical constraints, we may further shed light on the processes within the slab and during magma generation.

2. Geological setting

The Alaska Peninsula section of the Alaska-Aleutian subduction zone (AASZ) has a relatively constant convergence rate, direction, and plate age. This configuration has remained stable for the last 40–50 Ma, suggesting a uniform thermal state of the subducted slab along strike. Yet, substantial along-strike variations in seismicity are observed throughout the entire subduction zone. At shallow depths, megathrust earthquakes, including the 1938 M8.2 earthquake, occur every ~50–75 yr in the Semidi segment (Davies et al., 1981). In contrast, the "Shumagin seismic gap" stayed inactive for at least 200 yr until the M7.8 Simeonof earthquake on July 22, 2020 (Fig. 1). Geodetic observations reveal a transition of the seismogenic zone near the Shumagin Islands from dominantly creeping in the southwest to locked over a broad area in the northeast (Li and Freymueller, 2018). Intermediate-depth seismic activity also varies along strike (Shillington et al., 2015). A DSZ was discovered beneath the southwestern tip of the Alaska Peninsula, with a sharp end west of Shumagin Islands (Reyners and Coles, 1982; House and Jacob, 1983; Hudnut and Taber, 1987).

These along-strike variations generally coincide with the change in the pre-existing seafloor fabrics of the incoming Pacific plate. In the southwest, the incoming plate fabric makes a moderate angle with the trench, which correlates with abundant outer rise bending faults and lower velocities in the incoming plate uppermost

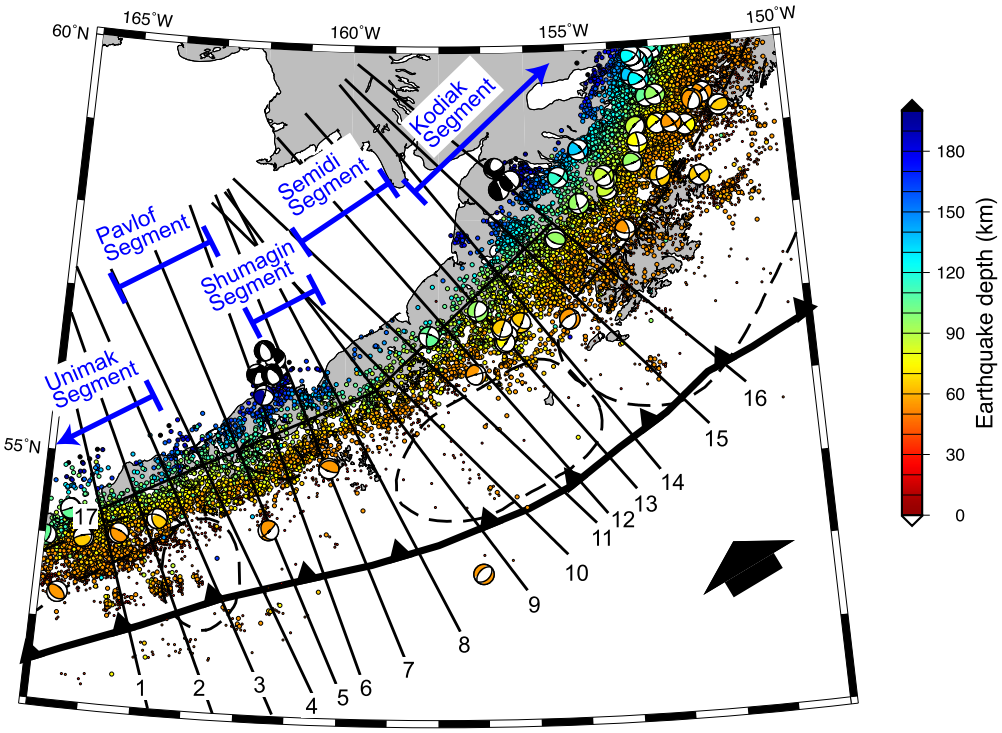

Fig. 2. Map of relocated intermediate-depth earthquakes from 1990 to 2018. Earthquakes (dots) are color-coded by depth. Focal mechanisms are determined by the Global CMT solutions (Ekström et al., 2012). Black lines illustrate the center of the 17 cross-sections in this study. The mid-points of cross-sections 1–16 are at the 75-km-depth contour of the Slab2 model (Hayes et al., 2018) spacing 50 km apart, except that the mid-points of #9 and #10 are 25 km apart. Each cross-section, numbered sequentially, is 111-km wide, 6° long, and perpendicular to the average strike of the Slab2 model at 50–100 km depths. Cross-section 17 is 500-km wide along the slab strike.

mantle compared to the northeast, where the incoming plate fabric is nearly trench-normal (Shillington et al., 2015) (Fig. 1). Based on these observations, Shillington et al. (2015) suggest that the fabric change near the Shumagin Islands, inferred from magnetic anomalies (Maus et al., 2009), enhances faulting and slab hydration before subduction and may control slab dehydration and earthquakes at depths. However, this fabric-control hypothesis is challenged by complex variations in intermediate-depth earthquakes and the recent M7.8 Simeonof megathrust earthquake.

In addition to the slab fabric change, sediment thickness and lithology vary along the strike of the Alaska Peninsula (Kelemen et al., 2003). A combination of locally derived turbidites, pelagic diatomaceous ooze, and relatively far traveled turbidites of the Zodiac fan enter the trench offshore. The Zodiac fan is a 280,000 km^3 headless deposit of turbidites originating potentially from British Columbia in the Eocene to Oligocene (Stevenson et al., 1983). The thickest sedimentary cover enters the trench between Veniaminof and Aniakchak (Fig. 1) with an average thickness of >300 m (Stevenson et al., 1983). East and west of this part, the Zodiac Fan pinches out, and pelagic sediments become increasingly dominated by younger diatomaceous ooze. Locally derived turbidites may also increase towards the eastern and western boundaries of our study area. However, they are largely absent at the Deep Sea Drilling Project (DSDP) site 183 (52.57°N, 161.21°W) southwest of Veniaminof, where a 505-m thick sedimentary sequence was drilled with ~200-m thick pelagic deposits of diatom-rich silty clay and diatom ooze overlying ~250-m thick Zodiac turbidites (Creager et al., 1973).

The volcanoes of the Alaska Peninsula have diverse eruptive histories and edifice characteristics that have been linked to magma chemistry and structural controls in the crust (Larsen, 2016). Our data analysis includes the Ukinrek Maars (~156.5°W) in the east. To the west, Aniakchak (~158°W), Black Peak (~158.8°W), and Veniaminof (~159.4°W) represent a cluster of volcanic systems that all experienced caldera forming eruptions in Holocene with numerous smaller eruptions more recently. Pavlof volcano (~161.9°W) is a steep stratocone and among the most active volcanoes historically in the Aleutians. Unimak Island with Shishaldin volcano (~164°W) represents the western boundary of our study area. Shishaldin has been part of prior along-arc investigations (Singer et al., 2007) and builds an important anchor for our analysis further east.

3. Intermediate-depth earthquakes

3.1. Data and earthquake relocation methods

We relocate intermediate-depth earthquakes between 1990 and 2018 with local magnitudes (M_L) ≥ 2.0 that were initially located by the Alaska Earthquake Center (AEC). We use local seismic arrival data (P and S phases) collected at the AEC stations and teleseismic P, S, pP, and sS arrivals from the International Seismological Centre database to constrain the absolute and relative locations. We also relocate 63 earthquakes earlier than 1990 from the Global Centroid Moment Tensor (CMT) catalog (Ekström et al., 2012) in the same region. It is worthwhile to note that multiple stations on the Aleutian Islands west of the Alaska Peninsula also recorded thousands of arrivals (Fig. S1a), assuring the relocation precision towards the west end of our study region.

We use an improved version of teletomoDD (Pesicek et al., 2010), a teleseismic double-difference relocation package with 3-D ray tracing, to relocate all the earthquakes. This method can utilize all local and teleseismic P, S, pP, and sS arrivals as well as a 3-D velocity model, thus can better constrain relative and absolute hypocenters. Due to the limited ray path coverage in the upper mantle, we only invert for the earthquake hypocenters and fixed the 3-D velocity model as known. We estimate relocation uncertainties with a bootstrap resampling approach. More details are described in Supplementary Text S1.

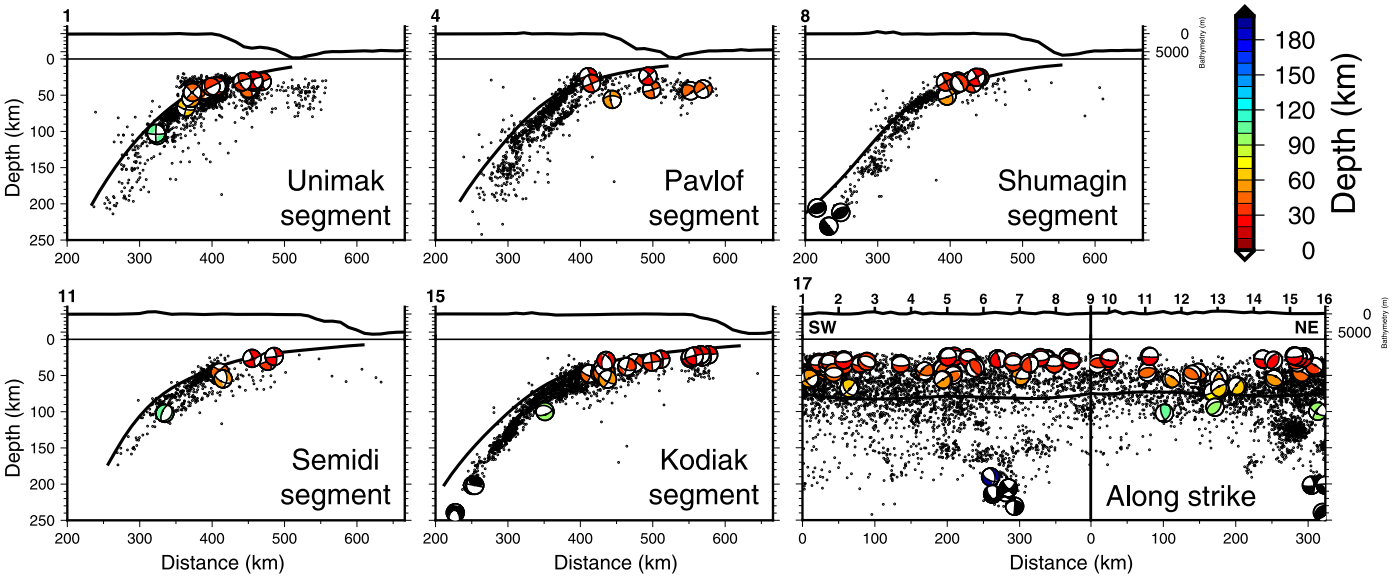

Fig. 3. Selected cross-sections of relocated earthquakes. Other cross-sections are shown in Fig. S3. Earthquakes are grouped into 5 segments based on their depth distributions shown in Fig. 4. Each of cross-sections 1–16 is 111-km wide and perpendicular to the average slab strike at 50–100 km depths, according to the Slab2 model (Hayes et al., 2018). Cross-section 17 is 500-km wide along the slab strike with all intersect cross-sections labeled on the top. The black curve in each panel indicates the slab top interface from the Slab2 model. The cross-section index number is at the top right corner of each panel. The bathymetry is plotted on top with vertical exaggeration. Focal mechanisms are color-coded by depth.

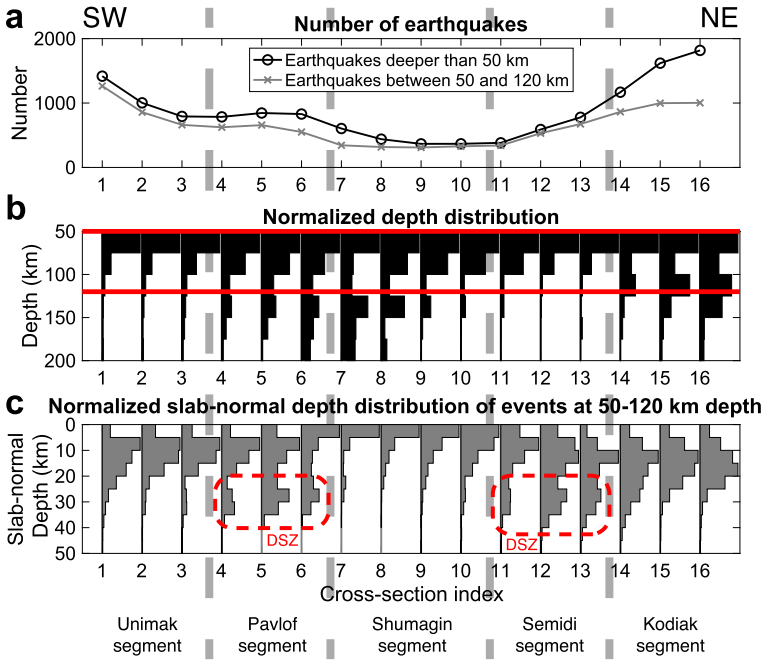

Fig. 4. Depth distributions of intermediate-depth earthquakes along all cross-sections. Vertical gray dashed lines illustrate the segment boundaries. (a) The number of intermediate-depth earthquakes deeper than 50 km (circles) and the ones at 50–120 km depths (crosses). (b) Vertical depth distribution. The number of events is normalized along each cross-section. Red lines show 50 and 120 km depths. (c) Slab-normal depth distribution of earthquakes at 50–120 km depths. Red dashed boxes highlight the double seismic zones (DSZs).

We further project all relocated earthquakes to 17 vertical cross-sections (black lines in Fig. 2) for further analyses (Fig. 3). The Slab2 model (Hayes et al., 2018) is used as the reference slab geometry. The mid-points of cross-sections 1–16 are chosen at the 75-km-depth contour spacing 50 km apart, except that the mid-point of cross-sections 9 and 10 are only 25 km apart. Each cross-section is 111-km wide, 6° long, and perpendicular to the average strike of the Slab2 model at 50–100 km depths. Along each cross-section, we analyze the number of intermediate-depth earthquakes and their vertical depth distribution. In order to identify DSZs, we also calculate the slab-normal depth distribution of earthquakes at 50–120 km depths (Fig. 4).

3.2. Earthquake distribution

More than 28,000 events with a 95% confidence in relative location smaller than 5 km in all directions are relocated. The median horizontal standard deviation is 0.45 km, whereas the median vertical standard deviation is 0.67 km (Fig. S2). About 21% of earthquakes are relocated shallower than 50 km and thus excluded in the following analyses. 152 events with the Global CMT solutions

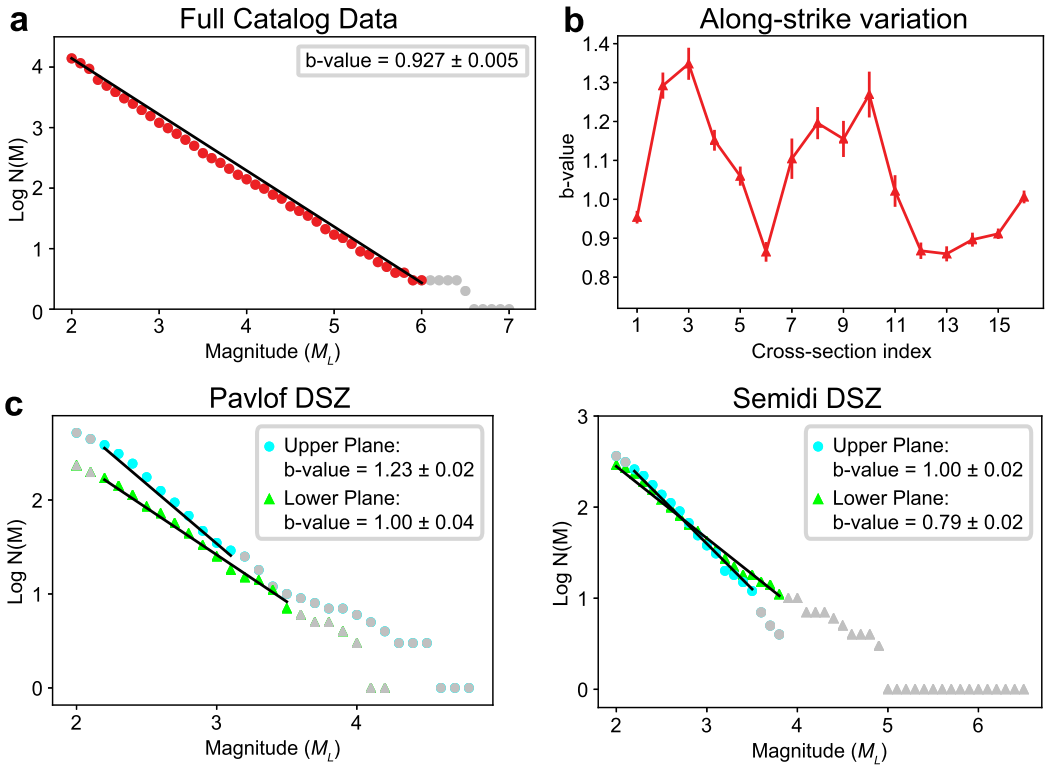

Fig. 5. Magnitude-frequency relationship of intermediate-depth earthquakes. (a) The accumulative number of earthquakes as a function of local magnitude (M_L) determined by the AEC in the study region. (b) *b*-values of intermediate-depth earthquakes along all cross-sections. Error bars indicate the 95% confidence intervals. (c) The accumulative number of earthquakes as a function of local magnitude (M_L) for the upper and lower planes of the Pavlof and Semidi DSZs. Gray symbols are not used for determining *b*-values.

(Ekström et al., 2012) are relocated. Many of them appear to be thrust events on the slab interface shallower than 50 km after relocating. It is important to note that the absolute number of earthquakes is controlled by not only local physical and geological properties but also detection capability. More events towards the northeast may simply reflect the higher detection capability near the mainland Alaska. We therefore focus on relative numbers along each cross-section.

Intermediate-depth earthquakes show significant along-strike variations in depth distributions (Fig. 2, Fig. 3, Fig. 4, and Fig. S3). According to their distribution, these earthquakes can be grouped into five segments from southwest to northeast: Unimak, Pavlof, Shumagin, Semidi, and Kodiak. In the Unimak segment, earthquakes concentrate in the upper 100 km depths, with a few extending to >150 km depths. The Pavlof segment is characterized by a clear DSZ at 50–120 km depths (Fig. 4c), which was initially discovered in the 1980s (Reyners and Coles, 1982; House and Jacob, 1983). Compared to its neighbors, the Pavlof segment has more earthquakes deeper than 100 km. Our results show a sharp eastern boundary of the Pavlof DSZ west of the Shumagin Islands, consistent with a previous study (Hudnut and Taber, 1987). The Shumagin segment has the least number of earthquakes in this region, which are almost confined above the 100 km depth and near the slab top interface. Earthquakes in the Semidi segment are also confined above the 100 km depth and form a DSZ, although the separation of the two planes is not as distinct as that of the Pavlof DSZ. The Kodiak segment has more earthquakes forming a single, thick layer extending to 200 km depth. We further confirm the Pavlof and Semidi DSZs with a variety of relocation algorithms and cross-section orientations (Supplementary Text S1).

Focal mechanisms of most intermediate-depth intra-plate earthquakes consistently show downdip extensional stress as suggested by previous studies (Reyners and Coles, 1982; House and Jacob, 1983). To the west of the Unimak Island (cross-section 1), a few events mark the transition of the slab stress state from downdip compressional along the Aleutian Arc to downdip extensional along the Alaska Peninsula (House and Jacob, 1983). The Global CMT solutions show that the upper planes of the Pavlof and Semidi DSZs consist of downdip extensional events. This is different from most DSZs in other subduction zones, suggesting that this part of the slab is overwhelmed by the downdip slab pulling force. Deepest earthquakes (~200 km) are found in the Pavlof and Kodiak segments, both showing maximum principle stress parallel to the slab strike, as a result of the slab along-strike contraction and downdip pulling (Ruppert, 2008).

3.3. Magnitude-frequency relationship (*b*-value)

Earthquake magnitude-frequency distribution can also reflect the nature of earthquakes. This distribution is commonly described by the Gutenberg-Richter law: $\log_{10}N = a - bM$, where N is the number of earthquakes with magnitudes equal to or larger than M, and a and b are both constants. Laboratory experiments and statistical analyses have demonstrated that high *b*-values of earthquakes are caused by lower stress of the source region (Scholz, 1968). For intermediate-depth seismicity, high *b*-values are usually attributed to fluids as the elevated pore fluid pressure can reduce the effective pressure and stress (Florez and Prieto, 2019).

We examine the magnitude-frequency relationship of intermediate-depth earthquakes and estimated the *b*-values along all cross-sections (Supplementary Text S3). All magnitudes are local magnitudes (M_L) determined by the AEC. The *b*-value of all intermediate-depth earthquakes in the entire region is 0.927 ± 0.005 (Fig. 5a), consistent with that of other subduction zones (Zhan, 2017). We also observe an along-strike variation of *b*-value from 0.86 ± 0.02 to 1.35 ± 0.04 (Fig. 5b). High *b*-values (>1.1) are generally found in the southeastern part of the study region (cross-sections 2–4 and 7–11). For the Pavlof and Semidi DSZs, the

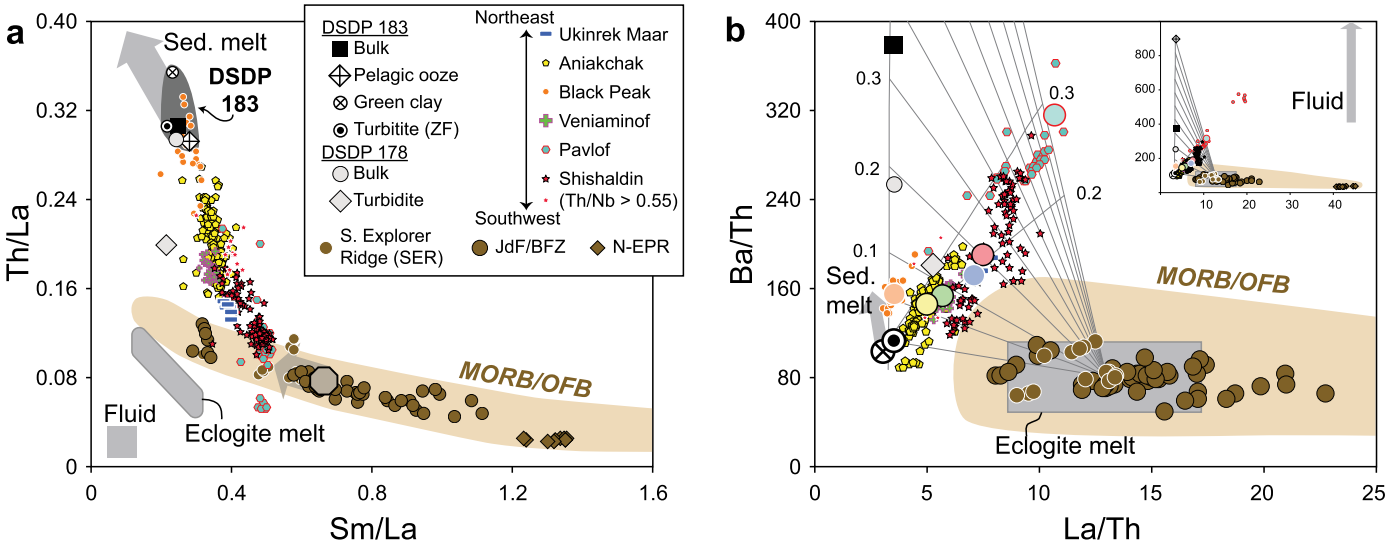

Fig. 6. (a) Th/La vs. Sm/La in magmas from the Alaska Peninsula, Deep Sea Drilling Program (DSDP) Sites 178 (offshore Alaska) and 183 (offshore Alaska Peninsula), mid-ocean ridge basalt/ocean floor basalt [MORB/OFB; from Jenner and O'Neill (2012)). Highlighted segments from the mid-ocean ridge and ocean floor basalt dataset include the Southern Explorer Ridge (SER, brown circles, white outline), the Juan de Fuca Ridge and Blanco Fracture Zone (JdFR/BFZ, brown circles, black outline), and the Northern Eastern Pacific Rise (N-EPR, brown diamonds). Eclogite melt is calculated following Yogodzinski et al. (2015) with the range corresponding to the enriched endmembers of JdF/BFZ and SER and a normal MORB as a depleted endmember (Sun and McDonough, 1989). Sediment melt and fluid are also calculated following Yogodzinski et al. (2015). See Supplementary Text S4 for Alaska Peninsula magma data. DSDP data include Zodiac Fan (ZF) turbidites from Plank and Langmuir (1998) and Plank (2014). (b) Ba/Th vs. La/Th. Symbols as in (a). Three-component mixing lines are calculated for the endmembers of pelagic ooze, Zodiac Fan turbidites, and a most depleted SER sample with La/Th ~ 13. Eclogite melt and the sub-arc mantle are similar and share the same characteristics. The inset shows the full data range including low Th samples from Pavlof and N-EPR. While fluid may have leverage for Ba/Th, its low concentrations in La and Th render its contributions small in most cases. Circles with lighter fill colors are average compositions for each volcano and referred to in the text. Sediment melt contributions following the arguments of Yogodzinski et al. (2015) would lead to higher Ba/Th than the bulk. The correlation of all volcano data and bulk sediment compositions suggests that Ba/Th is added equally from the sediments.

b-values of the upper planes are higher than those of the lower plane (Fig. 5c).

4. Trace elements of volcanic rocks

4.1. Geochemical tracers for variable sediment recycling

We use published geochemical major and trace element data of Alaskan igneous rocks to investigate slab dehydration and sub-arc melting beneath the Alaska Peninsula. Details about and constraints on the data as well as data filtering are described in Supplementary Text S4.

During crustal differentiation, Th is fractionated from the rare earth elements (REEs), resulting in elevated Th/La ratios in derivative subducted sediments. This Th enrichment relative to REEs correlates with known input sediment compositions in arcs worldwide (Plank, 2005). Given that Th and REEs are greatly enriched in sediments compared to the sub-arc mantle and underlying subducting basaltic crust, Th and REE budgets are strongly controlled by the subducting sediments. The volcanoes in the Alaska Peninsula show a remarkably consistent behavior for Th/La versus Sm/La (Fig. 6a). All centers form a coherent trend between bulk sediment compositions derived from DSDP 183 and a single mantle source (or fixed combination of mantle melts with other components). The mantle source here is represented by glass measurements from ocean floor basalts worldwide (Jenner and O'Neill, 2012) with basaltic glasses from the Southern Explorer Ridge (SER, ~49.6°N, 130.3°W) and the Juan de Fuca Ridge and Blanco Fracture Zone (JdFR/BFZ, 43.2-44.8°N, 127.5-130.4°W) specifically highlighted. The SER and JdFR/BFZ are the nearest active mid-ocean ridges to the Alaska Peninsula and may represent the oceanic crust that subducts underneath the Alaska Peninsula today based on current plate motions. Moreover, basalts from the Northern Eastern Pacific Rise (N-EPR) (~22.75°N, ~108.2°W) are shown to highlight a common depleted mid-ocean ridge basalt (MORB) mantle, which is the next closest active mid-ocean ridge region.

Sediment-dominated volcanic suites from Black Peak, Aniakchak, and Veniaminof fall close to the sediments at DSDP 183 and their derived melts (Plank and Langmuir, 1998). In particular, Black Peak is almost identical to the average DSDP 183 sediment (Fig. 6a). Pavlof, Shishaldin, and Ukinrek show a less prominent sediment signature. Their compositions extend the array towards a common endmember, which is a combination of the melts of the mantle wedge and of AOC in the form of eclogite melts. The latter is discussed in greater detail below and more details about the various components in the source magmas is presented in Supplementary Text S5. This endmember is slightly offset from the average SER-JdFR/BFZ basalt composition representing the mantle source to lower Sm/La in many geochemical discrimination diagrams in response to eclogitic contributions. Pavlof samples extend to a Th/La ratio below the mantle array. These samples have anomalously low Th concentrations compared to other trace element systematics, either related to a distinct contribution to magma genesis or potentially due to Th loss during sample preparation (0.4–0.5 ppm Th versus 0.75–1 ppm Th for most of the other Pavlof samples). Other highly incompatible elements (Cs/La, Rb/La, U/La; Fig. S4) show the same mixing array between the DSDP 183 bulk sediment and a restricted AOC plus mantle component. Black Peak is consistently the most enriched in the sediment component, followed by Aniakchak and Veniaminof. The centers with a smaller sediment signature vary in their rank. Most notably, Pavlof shows a slightly stronger sediment signature than Shishaldin compared to Th/La, further highlighting that the Th concentrations at Pavlof are somewhat anomalous.

Ba/La and Pb/La (Fig. S4) deviate from this general trace element pattern. Ba varies by a factor of ~5 in the two main lithologies in DSDP 183, pelagic diatomaceous ooze and turbidites of the Zodiac fan, while all other incompatible trace elements generally vary only by a factor of ~0.6–1.2, in particular, La varies by a factor of 0.68 (Plank and Langmuir, 1998). Consequently, Ba/La in clastic sediments such as turbidites associated with the Zodiac Fan (~35) is significantly lower compared to Ba-rich pelagic sediment of di-

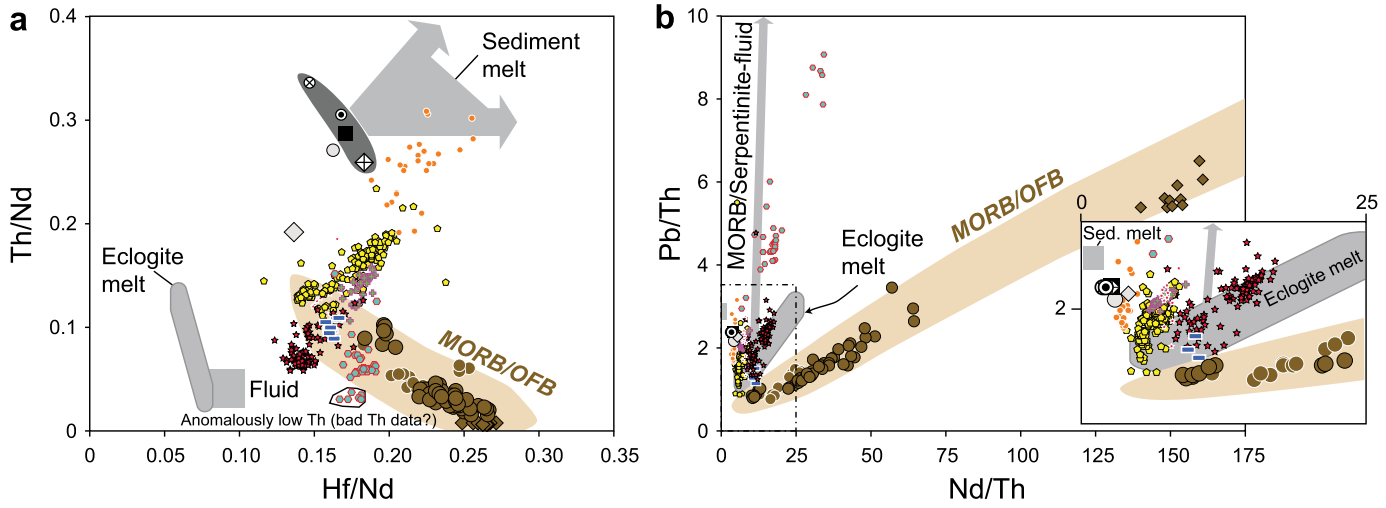

Fig. 7. (a) Th/Nd vs. Hf/Nd. Symbols as in Fig. 6a. Hf/Nd ratio for the eclogite and sediment melts from Yogodzinski et al. (2015), Th/Nd for the eclogite melt inferred from the data trajectory. Eclogite melt is calculated following Yogodzinski et al. (2015) with the range corresponding to the enriched endmembers of JdF/BFZ and SER and a normal MORB as a depleted endmember (Sun and McDonough, 1989). Sediment melt and fluid are also calculated following Yogodzinski et al. (2015). The calculated sediment melt represents a lower Th/Nd estimate (~0.43–0.51) than high Th/Nd for sediment melt has been proposed by Class et al. (2000; Th/Nd sediment melt ~0.6) and Singer et al. (2007; Th/Nd sediment melt ~1.1). (b) Pb/Th vs. Nd/Th. Sediment and eclogite melts are displaced to low Pb/Th and low Nd/Th. Specifically, Aniakchak and Black Peak show this signature. High Pb/Th, in particular for Pavlof and, to lesser extent, Shishaldin, cannot be explained by sediment and eclogite melts in addition to the arc mantle source (generally similar to the MORB/OFB array). An additional Pb component likely represents slab fluids, either from MORB or underlying serpentinite. Inset: Zoom-in of the low Pb/Th and low Nd/Th region of the diagram showing sediment and eclogite melts as well as data trends from the bulk sediment composition towards these endmembers.

atomaceous ooze (~260). In fact, the average Ba/La of 115 in DSDP 183 is significantly higher than the Ba/La value (~50, Black Peak) in lavas with the strongest sediment signature derived from other incompatible elements. The array of magma compositions for the Alaska Peninsula is significantly less coherent than the other mixing diagrams. This suggests that sediment contributions to the arc lavas are a combination distinct from the average DSDP 183 composition.

Ba/Th ratios are uniquely sensitive to the type of sediment input present along strike the Alaska Peninsula and may reveal the relative contributions from turbidites and pelagic ooze. Ba/Th is best constrained when compared to La/Th (Fig. 6b). Linear combinations in this diagram are mixing lines because of the common denominator Th. In addition to turbidites and pelagic ooze, the third component (AOC + mantle) is estimated from the intercept with the mantle array from Fig. 6a with a La/Th ratio of ~13. Although this ratio is not well constrained given the small variations in Th/La of the mantle array, its co-location with trace element ratios for eclogite melt further strengthen this end-member composition (see Supplementary Text S5 for details). The sediment component for all magmas in the Alaska Peninsula is dominated by clastic sediments described as turbidites and green clay equivalent to the Zodiac Fan. All datasets for each volcano trend towards this endmember, with Black Peak, Aniakchak, Veniaminof receiving their sediment signature almost exclusively (>9:1) from the turbidites and green clays. The Ukinrek Maars samples and the average composition of Shishaldin have a contribution from turbidites to the sediment signature 80–90%. However, Shishaldin samples show the largest variations in Ba/Th with a factor of ~2, and therefore the turbidite contribution may range between ~50–95%. Some of this variability is independent of La/Th and only expressed in Ba/Th, which may represent a superimposed fluid signature. Pavlof shows the largest contributions of pelagic ooze to the sediment signature (up to 100%). The anomalously low Th samples from Pavlof fall outside of the mixing triangle. Except for Shishaldin and Pavlof, the relative sediment contributions of turbidite/green clay versus pelagic ooze are relatively insensitive to the choice of the AOC + mantle endmember. Some uncertainties may be introduced by looking at magma compositions that exceed 60 wt.% SiO_2 (Fig. S5, Fig. S6, and Fig. S7). Lastly, Ba/Th has been conventionally interpreted to be a fluid signature (e.g., Hawkesworth et al., 1997), but the low mobility of Th and REEs in fluids would require very large contributions from fluids that can be simply accommodated by a changing sediment melt source for most samples. As noted above, an exception shows that the primitive samples of Shishaldin (Fig. 6b and S7) follow a trajectory to high Ba/Th at a nearly constant La/Th value, possibly indicating fluids. Whether Pavlof also follows such a superimposed fluid trajectory is unclear as it may be biased by the samples for which we question the reported Th concentrations.

It is noteworthy that while Th/La consistently tracks sediment input, it misses significant sediment contributions for Pavlof and Shishaldin, a phenomenon also reported by Plank (2005) for other arcs. Therefore, at the Alaska Peninsula, Ba/Th is primarily an effective signature to unravel the different sediment inputs rather than a fluid signature, which others have also cautioned (Hermann and Rubatto, 2009).

4.2. Sediment contributions and the role of AOC

Previous studies in the Aleutians have argued that the sediment contribution is in the form of a melt based on isotope systematics combined with geochemical tracer such as Th/Nd, which behaves similarly to Th/La (e.g., Class et al., 2000; George et al., 2003; Singer et al., 2007). These studies inferred a sediment melt with high Th/Nd (~0.4–0.5 to ~1.1). Constrained by sediment melting experiments, Yogodzinski et al. (2015, their Fig. 18) showed that sediment melts are also enriched in Hf relative to Nd. Moreover, they demonstrated that eclogite melts of AOC are low in Hf/Nd as Hf tracks residual garnet and zircon (see Supplement Text S5 for details). Thus, in the absence of isotopes, the Th/Nd versus Hf/Nd systematics may reveal the relative importance of sediments and their melts as well as eclogite melts of AOC.

Magma compositions from the Alaska Peninsula require contributions from sediment and eclogite melts (Fig. 7a). Fluids may have similar Th/Nd and Hf/Nd characteristics, but their low carrying capacity of these elements make fluids less likely to control the source compositions here. A coherent trend of a two-component

mixing between a sediment melt component with Hf/Nd >0.2 and high Th/Nd and an eclogite melt component with low Th/Nd and low Hf/Nd explain the variance in the data with small modifications by the sub-arc mantle represented by lavas from JdF/BFZ and SER. Consistent with previous observations, we find the largest contributions of sediment melt in samples from Black Peak, Aniakchak, and Veniaminof. In contrast, eclogite melt contributions are most pronounced in magmas from Shishaldin, Pavlof, and Ukinrek. Pavlof is the only center that falls off the main trend, potentially related to a larger contribution from a depleted mantle source. Especially, the low Th samples require a depleted mantle source, similar to the N-EPR with low Th/Nd but high Hf/Nd characteristics.

4.3. Potential fluid indicators

Although trace element systematics suggest a predominance of four melt components (turbidites, pelagic ooze, eclogite, and sub-arc mantle) contributing to magmas in the Alaska Peninsula, minor variance in the data may be related to fluids. While Ba variations can be explained primarily using sediment and eclogite melt proportions (Fig. 6), Pb in Alaskan magmas requires additional contributions, potentially fluids, which have been long recognized [e.g., by exploring Ce/Pb (Miller et al., 1994)].

We explore Pb and potential fluid contributions using Pb/Th vs. Nd/Th (Fig. 7b, see also Pb/La in Fig. S4), with Nd/Th being linked closely to contributions from sediment and eclogite melts (Fig. 7a). Our model for eclogite melt uses compositions of the oceanic crust not affected by potential Pb loss due to hydrothermal leaching (e.g., Peucker-Ehrenbrink et al., 1994) and thus may represent a maximum Pb/Th in eclogite melts (see Supplementary Text S5 for details). Most volcanic centers cluster at low Pb/Th and low Nd/Th pointing to an enriched eclogite (i.e., JdF/BFZ and SER) and/or mantle source. A separate vector in the data that cannot be reconciled with just sediment and eclogite melts is found in samples from Pavlof and to a lesser extent from Shishaldin with high Pb/Th and elevated Nd/Th. For Shishaldin, a more depleted eclogite/sub-arc mantle would have to be invoked to explain the higher Nd/Th. Therefore, any magma that is enriched in Pb (high Pb/Th) beyond the sediment signature and falls outside of a ternary mixture of sediment melt, eclogite melt, and sub-arc mantle requires an additional component, presumably fluids. This deviation is most evident for Pavlof samples. At Shishaldin, the fluid signature is not strongly expressed in Pb/Th, but together with the observation of a trajectory in Ba/Th, suggesting that Shishaldin also contains a stronger fluid signature.

5. Fluids and sediments in the subducting slab

5.1. Slab dehydration revealed by intermediate-depth seismicity and trace elements

High Pb/Th ratio along with low Th/La indicate high fluid contributions from MORB crust or serpentinized mantle of a subducted slab (Scambelluri et al., 2019). In addition, it is generally agreed that intermediate-depth intra-plate earthquakes are related to dehydration reactions within the subducted slab (e.g., Hacker et al., 2003; Yamasaki and Seno, 2003). Although the absolute number of intermediate-depth earthquakes depends on a variety of factors, including the slab stress state, hydration status, and detection capability, the relative distribution of these earthquakes has been widely used as a proxy for slab-derived fluids. More earthquakes at greater depths may imply more water subducted to those depths (Wei et al., 2017), and more earthquakes in the slab interior beneath the slab Moho generally suggest more dehydration in the slab mantle.

High *b*-values of intermediate-depth earthquakes are also indicative of fluids. Studies in the Alaska, NE Japan, and New Zealand subduction zones show high *b*-values (>1.2) coinciding with seismic low-velocity anomalies that indicate fluids released from slab dehydration and magma in the overriding plate (Wiemer and Benoit, 1996; Wyss et al., 2001). For DSZs in multiple subduction zones, the *b*-value of the upper-plane seismicity appears to be consistently higher than that of the upper-plane events (Florez and Prieto, 2019), suggesting more fluids near the slab surface. One exception is observed in the Tohoku DSZ, where the lower plane has a higher *b*-value compared to the upper plane (Kita and Ferrand, 2018).

At the Alaska Peninsula, intermediate-depth seismicity and chemical signatures of arc magma indicate along-strike variations of fluid distribution in the slab and slab dehydration (Fig. 8e). In the Unimak segment, a 30-km-thick seismic zone at 50-100 km depths, few earthquakes deeper than 100 km, high *b*-values (>1.2), and high Pb/Th (2.2 ± 0.5) with low Th/La (0.14 ± 0.03) in Shishaldin magmas all suggest that slab dehydration extends from the slab crust to ~20 km beneath the slab Moho and is mostly confined above the 100 km depth. In the Pavlof segment, a DSZ extends from the slab crust to 30 km beneath the slab Moho, the *b*-value of the upper plane is among the highest (~1.2), more earthquakes extend to depths greater than 100 km, and the Pb/Th ratio (5.1 ± 1.7) at Pavlof is significantly higher than that at other volcanoes, while Th/La is the lowest (0.10 ± 0.03). These all suggest that the slab dehydration extends to ~200 km depth and also the inner part of the slab mantle. In the Shumagin segment, most earthquakes with high *b*-values (1.1–1.3) are confined to <100 km depth and within the slab crust, suggesting high water content and thus more extensive dehydration near the slab surface. This is consistent with the relatively low Pb/Th ratio (2.1 ± 0.1) in relation to elevated Th/La (0.18 ± 0.01) at Veniaminof. In the Semidi segment, the DSZ implies that slab dehydration may occur in the slab interior. However, the lower Pb/Th ratios (1.8–2.0) with high Th/La (0.20–0.28) at Aniakchak and Black Peak suggest less fluid in this segment compared to the Pavlof segment. Moreover, the moderate *b*-values (1.0 for the upper plane and 0.8 for the lower plane) and few earthquakes deeper than 100 km also suggest that slab dehydration is restricted and does not extend to greater depths. The Kodiak segment has a thick seismic zone extending to ~200 km depth with moderate *b*-value (0.9–1.0) and the lowest Pb/Th ratio (1.3 ± 0.2) and relatively low Th/La (0.14 ± 0.01) at Ukinrek, suggesting that moderate slab dehydration extends ~20 km into the slab mantle and to ~200 km in vertical depth.

In sum, slab dehydration appears to be most extensive in the Pavlof segment in both slab-normal and vertical directions (Fig. 8a and Fig. 8b). Additionally, *b*-values of these events and Pb/Th ratios of arc magma suggest that the slab dehydration is more intensive in the southwest compared to that in the northeast (Fig. 8c). The presence of slab fluids is consistent with previous geochemical studies for Shishaldin (Singer et al., 2007). The fluids are likely derived from the subducting slab crust and serpentinized mantle at depths, which have been imaged in the Japan subduction zone with extensive seismic data (Zhang et al., 2004; Nakajima et al., 2009). Seismic images beneath the outer rise of the Semidi segment suggest that the crust and uppermost mantle of the incoming plate are hydrated through bending faults (Shillington et al., 2015). More high-resolution seismic images of the Alaska slab from the trench to great depths will reveal the relationship between the serpentinized mantle beneath the outer rise and the slab mantle dehydration at depths greater than 50 km. High *b*-values (>1.0) are generally associated with earthquakes near the slab surface in the Unimak and Shumagin segments, where events concentrated within the top 15 km from the slab surface. In contrast, the *b*-values of earthquakes in the slab interior are relatively (<1.0) low

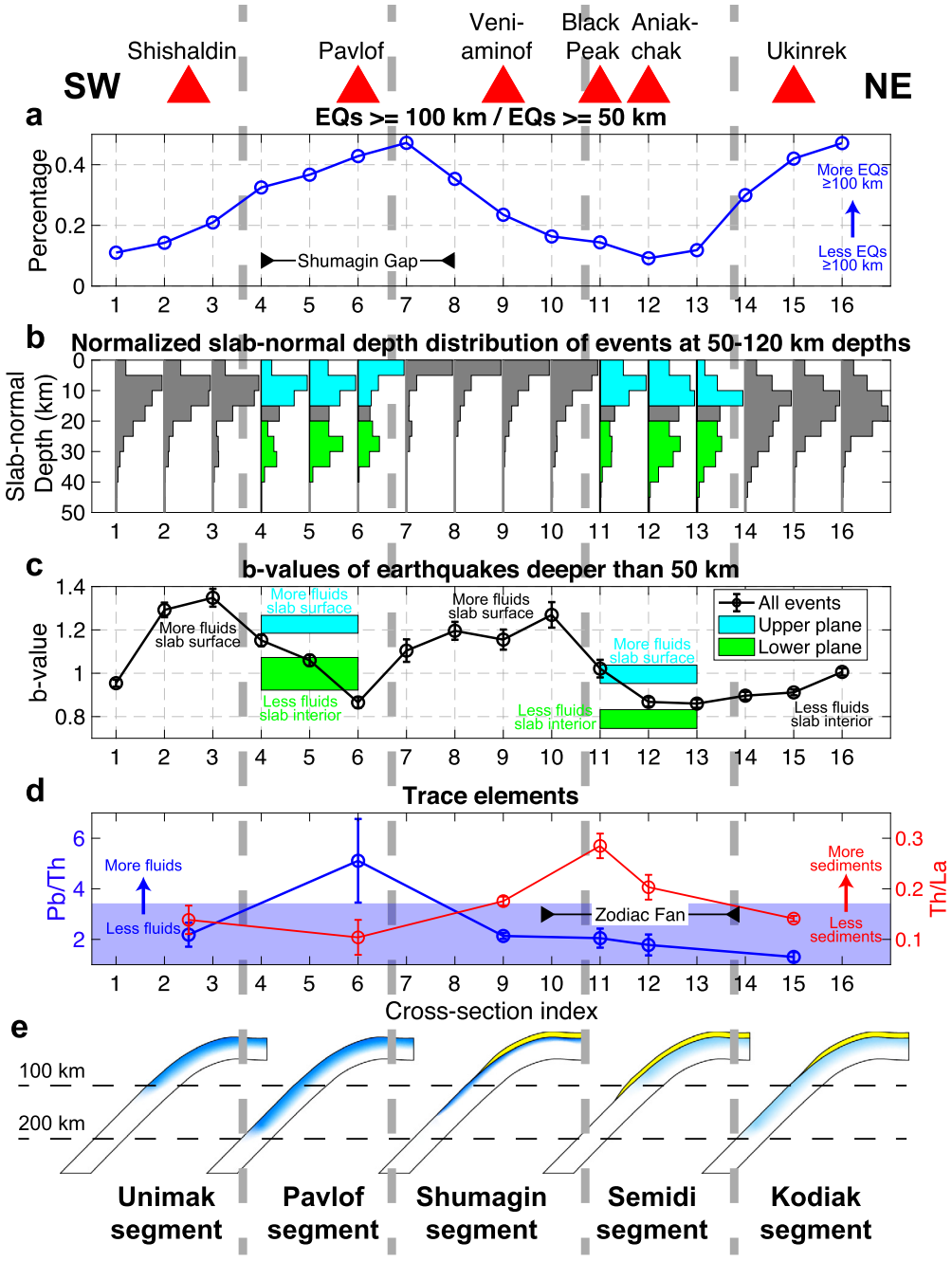

Fig. 8. Spatial correlation among earthquake parameters and geochemical proxies along all cross-sections. Selected volcanoes are plotted at the top, whereas segment names are shown at the bottom. (a) The number of earthquakes deeper than 100 km compared to all intermediate-depth events (> 50 km). (b) Slab-normal depth distribution of earthquakes at 50–120 depths from Fig. 4c. Cyan and green illustrate the upper and lower plane of the DSZs, respectively. Note that the Slab2 model (Hayes et al., 2018) introduces a systematic shift of earthquakes relative to the slab surface along certain cross-sections. (c) *b*-values of intermediate-depth earthquakes along all cross-sections, the same as Fig. 5b. Cyan and green boxes indicate the *b*-values of the DSZ upper and lower planes, respectively, with their vertical widths showing the 98% confidence intervals. (d) Th/La (red) and Pb/Th (blue) ratios from selected volcanoes as proxies of subducted sediments and fluids, respectively. The blue shade area indicates the Pb/Th values that can be explained by sediment and eclogite melts without invoking fluids according to Fig. 7. Pavlof shows a strong fluid signature, whereas other volcanoes in the northwest show low fluid concentration. The fluid signature at Shishaldin is elusive based on the existing Ba and Th data (see details in section 4.3). (e) Cartoons (not to scale) illustrating the slab dehydration and sediments based on the along-strike variations in the above panels. Blue to cyan colors indicate high to low level of slab dehydration. The yellow layer on top of the slab represents the subducted sediments.

in the Kodiak segments, where the majority of earthquakes are in the slab mantle. In addition, *b*-values for the DSZ upper-plane earthquakes are consistently higher than those for the lower-plane events, in agreement with the previous global survey (Florez and Prieto, 2019), implying a dryer lower plane compared to the upper plane. The existence of a DSZ does not correlate with a high *b*-value for either the upper or lower plane, suggesting that fluids are not the predominating factor in developing a DSZ. Instead, the local stress state within the slab is probably more important in triggering earthquakes in the lower plane.

5.2. Sediments revealed by trace elements and plate slip deficit

It has been long recognized that thorium (Th) is an excellent tracer of sediment input into a subduction zone (e.g., Plank, 2005). Along-strike variations in Th/La suggest variable input of subducted

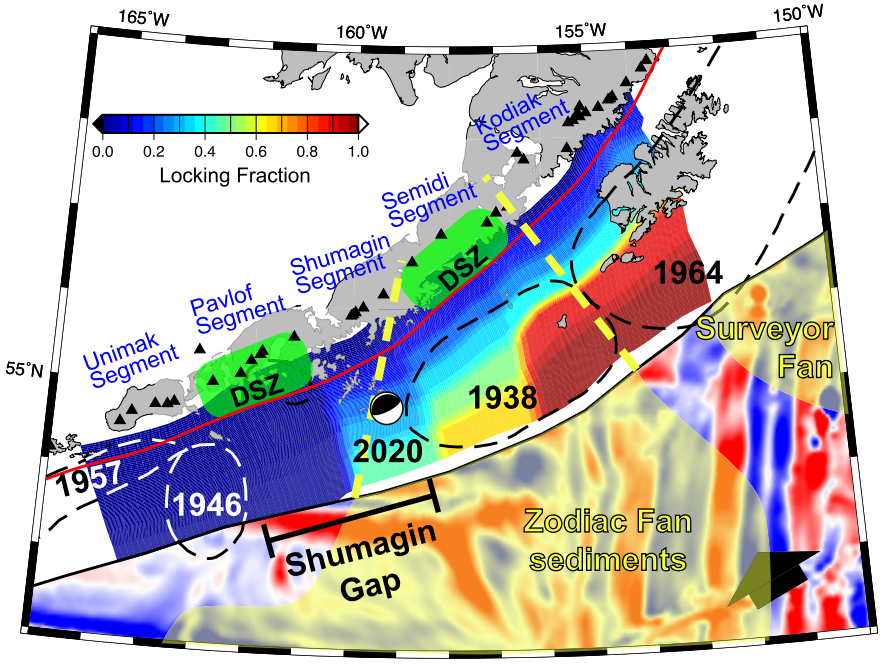

Fig. 9. Along-strike segmentation of the Pacific slab beneath the Alaska Peninsula. The red curve indicates the 50-km depth contour of the slab surface, roughly delineating the boundary between intra-plate intermediate-depth seismicity and inter-plate seismogenic zone at shallow depths. Green boxes outline the identified Pavlof and Semidi DSZs, that divide the slab at intermediate depths (50–200 km) into 5 segments (blue texts). Red to blue polygons show the plate coupling model from locking to creeping based on geodetic observations (Li and Freymueller, 2018). The pre-existing fabrics of the incoming plate are represented by seafloor magnetic anomalies (Maus et al., 2009) on the Pacific Plate. The yellow dashed lines illustrate the subducted Zodiac Fan sediments inferred from the Th/La ratios in Fig. 8d. Other features are the same as Fig. 1.

sediments along the Alaska Trench (Fig. 8d). The highest Th/La ratios in the Semidi segment indicate the subducted Zodiac Fan sediments down to at least 100 km depth. In contrast, the low Th/La ratios in the Unimak and Pavlof segments suggest significantly less sediment subducted to this depth. Towards the southwest, the influence of the Zodiac Fan vanishes, and any sediment input becomes increasingly dominated by pelagic diatomaceous ooze (Fig. 6b).

In the seismogenic zone above 50 km depth, subducted sediments can smooth the plate interface, enhancing plate coupling and facilitating megathrust earthquakes (e.g., Ruff, 1989). In the Alaska Peninsula section of the AASZ, the along-strike variation of sediments in the seismogenic zone can be roughly revealed by plate slip deficit constrained by geodetic observations (Fig. 9). In Pavlof and Unimak segments, the subducting plate is nearly decoupled from the overriding plate. In contrast, two plates are fully locked in the Kodiak segment (Li and Freymueller, 2018), coinciding with the subduction of Zodiac and Surveyor sedimentary fans (von Huene et al., 2012). This is in good agreement with the change in Th/La ratio that samples the sediments at great depths, suggesting more sediments input in the northeast.

The recent M7.8 Simeonof earthquake ruptured the shallow part of the Shumagin segment, which had been seismically inactive for at least 200 yr. It is unclear whether the rupture extended into the Pavlof segment. Therefore, the Shumagin segment appears to be a transitioning point that separates the fluid-rich, sediment-poor southwestern segments from the fluid-poor, sediment-rich northeastern segments.

5.3. Depletion of Nb in subduction zones

A fundamental characteristic signature of arc magmas is the depletion of Nb (and Ta) relative to similarly incompatible elements (e.g., Ce). It remains an unresolved question (Plank, 2014) whether the low Nb/Ce signatures in arc magmas are mostly inherited from continents through bulk involvement of subducting sediments or

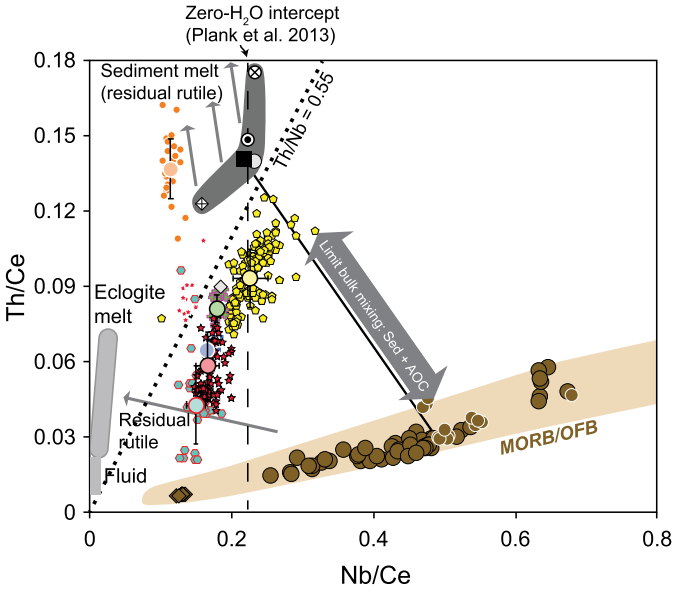

Fig. 10. Th/Ce vs. Nb/Ce. Symbols as in Fig. 6a. Large colored circles are the averages for each magmatic center. Bulk mixing between sediment and altered oceanic crust (AOC) is shown as a limit for the highest possible Nb/Ce, assuming that the SER and JdFR present good endmembers for the AOC. Melting of sediment or eclogite, if rutile-bearing, is displaced to low Nb/Ce in case of residual rutile. The dashed line is the inferred Nb/Ce ratio assuming a zero-H_2O intercept for primitive magmas in the Aleutians from Plank et al. (2013).

further enhanced during melting in subduction zones in the presence of residual rutile, which retains Nb (Hermann and Rubatto, 2009). Since our and other geochemical studies (e.g., Class et al., 2000; George et al., 2003; Singer et al., 2007) using Th/Nd have shown that the sediment contribution is primarily in the form of a sediment melt (Fig. 7a), we can explore the role of residual rutile for this segment of the arc using Th/Ce vs. Nb/Ce (Fig. 10), with Th/Ce replacing Th/La and Th/Nd to retain the same denominator.

We have argued that many trace element signatures point towards an eclogite melt endmember that is similarly enriched like the SER and JdFR (Section 4.1). This is consistent with the low Sm/La data for Shishaldin (Singer et al., 2007) that reveal a more enriched mantle + AOC endmember compared to volcanoes west of Shishaldin. Moreover, published $^{143}Nd/^{144}Nd$ ratios of ~0.5131 in basalts from the SER and JdFR (Hegner and Tatsumoto, 1987; Cousens et al., 2017) are consistent with the mantle + AOC isotope compositions for Shishaldin magmas (Singer et al., 2007), and plate motion today suggests that these mid-ocean ridge segments project towards the Alaska Peninsula. However, we note that a commonly depleted endmember cannot be rejected at this point. Therefore, our preferred enriched source represents an upper limit for any Nb/Ce in magmas from the Alaska Peninsula when considering bulk mixing of sediment and mantle + AOC. A lower limit for mantle + AOC may be represented by samples from the N-EPR. We reject this composition as an endmember for Alaskan volcanoes because it would require bulk mixing of DSDP 183 sediments and mantle + AOC to produce the magmas of Ukinrek, Aniakchak, Veniaminof, Shishaldin (low Th/Nb set), and Pavlof. While Aniakchak would even require preferential addition of Nb from sediments to extend Nb/Ce beyond the composition of bulk sediment nearby, Black Peak would require Nb retention.

Instead, we argue that residual rutile during sediment melting and eclogite melting enhances the low Nb/Ce ratio in the Alaska Peninsula. Depending on the slab thermal condition and the sediment thickness, Nb is variably added during magma genesis alongstrike, and most efficiently under Aniakchak and Veniaminof. The Th/Ce vs. Nb/Ce systematics show the need for further constraints of the mantle + AOC component to fully understand and quantify Nb systematics (Fig. 10).

These findings regarding Nb/Ce in the Alaska Peninsula have important implications for water estimates in arc magmas of the AASZ. A recent compilation of water contents in AASZ magmas (Plank et al., 2013) presented an anti-correlation between H_2O/Ce and Nb/Ce, supporting the hypothesis that volatile contents measured in melt inclusions represent primitive arc magma water contents. However, the H_2O/Ce-Nb/Ce relationship projects to Nb/Ce of ~0.22 for quasi-dry magmas. This implies that magmas from Aniakchak and to a lesser extent from Veniaminof would be almost water-free, a prediction that contradicts their explosive eruptions. Shishaldin has the next highest Nb/Ce of the studied volcanoes and has a direct water measurement from melt inclusions [~2 wt.% (Plank et al., 2013)]. It was one of the volcanoes for which the H_2O/Ce-Nb/Ce relationship was derived. However, those contents were determined in evolved olivine (~Fo_{72}), potentially limiting the use of constraining primitive water contents. These considerations question the simple anti-correlation between H_2O/Ce and Nb/Ce. Instead, higher water contents may be permissible in some of these primitive magmas (Gavrilenko et al., 2019).

5.4. Controlling factors on along-strike variations

Our results are generally consistent with the fabric-control hypothesis (Shillington et al., 2015), suggesting that the fabric orientation and slab hydration at the outer rise have a lasting impact on intermediate-depth seismicity and sub-arc melting. The Pavlof segment has the greatest extent of slab dehydration at great depths, whereas the Semidi segment has the least water subducted beyond 50 km depth (Fig. 8e). The incoming plate in the Pavlof segment is more hydrated because the seafloor fabrics are sub-parallel to the trench and thus easier to open as outer rise bending faults. After being subducted to shallow depths (<50 km), more water is released from the subducted sediments and upper crust to facilitate plate creeping. Beyond 50 km depths, more hydrous minerals in the slab crust and mantle break down, releasing water to facilitate hydrous flux melting and trigger more intermediate-depth earthquakes. In contrast, the incoming plate in the Semidi segment is less hydrated because of the orientation of the seafloor fabrics; the slab thus experiences less dehydration at all depths, resulting in more plate coupling and weaker seismic activity.

However, our results also show more complexities beyond the fabric-control hypothesis that only considers water stored in the plate-bending faults. First, although the Unimak, Pavlof, and Shumagin segments of the subducting plate share the same fabric orientation and the high water content inferred from *b*-values, the extent of slab dehydration varies significantly (blue shades in Fig. 8e). Particularly, the sharp boundary of plate coupling from creeping to partially locking west of the Shumagin Islands coincides with the eastern boundary of the Pavlof DSZ. This suggests that fabric orientation is not the only factor controlling the slab hydration state. The subducted sediments may serve as a cover impeding more water penetrating into the slab interior of the Shumagin segment. Alternatively, if the lower plane of the Pavlof DSZ is caused by carbonate-related shear instability (Kirby and Kelemen, 2019), the contrast between the Pavlof and Shumagin segments then reflect the change in carbonate rather than water within the slab. Second, in the Semidi and Kodiak segments, the subducted sediments appear to be more important than water. The thick Zodiac and Surveyor sedimentary fans not only smooth and lock the plate interface, but also contribute to the sub-arc melting. Third, intra-plate seismicity extends to ~200 km depth in the Pavlof and Kodiak segments but not the others, although the thermal parameter is nearly constant across the region. This variation conflicts with the hypothesis that the maximum depth of intermediate-depth seismicity is mainly controlled by the slab thermal state because serpentine dehydration reactions are most sensitive to temperature (Wei et al., 2017). The slab stress state may play a more important role in affecting the maximum depth of intermediate-depth seismicity beneath the Alaska Peninsula. Further investigations, particularly high-resolution seismic tomography of the slab and volatile measurements of melt inclusions, are needed to explore the distribution of fluids and sediments in the slab.

6. Conclusions

We analyze the distribution and magnitude-frequency relationship of intermediate-depth intra-plate earthquakes and trace elements of arc lavas in the Alaska Peninsula. Our results show five distinct segments of the slab deeper than 50 km along strike from southwest to northeast (Fig. 8e and Fig. 9):

Unimak: A 15-km-thick seismic layer with high *b*-values (>1.2) extends to about 100 km depth. Arc lavas are characterized by low Th/La (0.14 ± 0.03). The relatively high Pb/Th value (2.2 ± 0.5) and a nearly vertical trend in the Ba/Th-La/Th diagram may indicate fluids in addition to sediment and eclogite melts in the arc magma source region. These imply that the slab dehydration occurs in the slab crust and uppermost mantle down to 100 km depth, and there is little sediment subducted to this depth.

Pavlof: A 35-km-thick seismic layer extends to about 200 km depth, and a DSZ exists at 50–120 km depths. The upper plane of the DSZ has high *b*-values (~1.2). Arc lavas have the lowest Th/La (0.10 ± 0.03) but highest Pb/Th (5.1 ± 1.7) in the region. The slab dehydration appears to occur in the slab crust and uppermost mantle down to 200 km depth, and there is little sediment subducted to the sub-arc melting source. The distinct two planes of the DSZ probably suggest that the slab internal stress due to plate unbending drives fluids to these two regions.

Shumagin: Most earthquakes with high *b*-values (1.1–1.3) are confined in the slab crust and above 150 km depth, and the Th/La (0.18 ± 0.01) and Pb/Th (2.1 ± 0.1) ratios of arc lavas are moderate. The slab dehydration is confined primarily in the slab crust down

to 150 km depth and there are moderate sediments subducted to the sub-arc melting source.

Semidi: A 40-km-thick DSZ with moderate *b*-values of the upper plane (~1.0) extends to about 100 km depth. Th/La (0.20–0.28) is the highest in the region, whereas Pb/Th (2.0–2.2) is low. We suggest that the slab dehydration is less intensive compared to the southwestern segments and occurs in the slab crust and uppermost mantle down to 100 km depth, and there are significant Zodiac Fan sediments subducted to the sub-arc melting source. Although the fluid concentration here is allegedly lower than that in the Pavlof and Shumagin segments, the slab internal stress still drives fluids to form a DSZ.

Kodiak: Most earthquakes with low *b*-values (0.9–1.0) occur in the slab mantle down to 200 km depth, and Th/La (0.14 ± 0.01) is moderate with the lowest Pb/Th (1.3 ± 0.2), implying that fluids distribute widely in the slab mantle down to 200 km but with a low concentration. Although there are significant amounts of sediments subducted to about 50 km depth, they appear to not reach the sub-arc melting source region.

This segmentation suggests that the slab dehydration and sub-arc melting vary along strike, primarily controlled by the water and sediments subducted with the slab. More water is subducted in the southwest whereas more sediments in the northeast. This transition is probably influenced by the change in the orientation of pre-existing fabrics in the incoming plate as well as the subduction of the Zodiac sedimentary fan. More intriguingly, the slab segmentation deeper than 50 km inferred from our results remarkably coincides with the plate slip model shallower than 50 km (Li and Freymueller, 2018). This coincidence suggests that the along-strike variations in the slab affect seismicity and mantle melting from the trench to great depths.

CRediT authorship contribution statement

S. Shawn Wei: Conceptualization, Methodology, Formal analysis, Visualization, Writing – Original Draft, Writing – Review & Editing, Supervision, Project administration, Funding acquisition. **Philipp Ruprecht**: Methodology, Formal analysis, Visualization, Writing – Original Draft, Writing – Review & Editing, Supervision, Funding acquisition. **Sydney L. Gable**: Methodology, Formal analysis, Visualization, Writing – Review & Editing. **Ellyn G. Huggins**: Geochemical data compilation and analysis, Writing – Review & Editing. **Natalia Ruppert**: Data Curation, Writing – Review & Editing. **Lei Gao**: Software, Writing – Review & Editing. **Haijiang Zhang**: Methodology, Software.

Declaration of competing interest

The authors declare that they have no known competing financial interests or personal relationships that could have appeared to influence the work reported in this paper.

Acknowledgements

We thank C. Drooff, Y. Huang, J. Freymueller, D. Rasmussen, D. Shillington for constructive discussions, F. Wang for helping with data processing, and two anonymous reviewers for helpful comments. T. Plank is particularly thanked for insights on the relationship between Th and Nb in volcanic rocks. We also thank Rebecca Bendick for her excellent editorial handling. We greatly appreciate the open access of whole rock data provided by the Alaska Volcano Observatory and would specifically like to thank K. Wallace for the Veniaminof data. This work was made possible by NSF grants OCE-1842989 to S.S.W. and EAR-1426820/1719687 to P.R. S.S.W. was also supported by the MSU Geological Sciences Endowment. Seismic traveltime data are available at the Alaska Earthquake Center and the International Seismological Centre.

Appendix A. Supplementary material

Supplementary material related to this article can be found online at https://doi.org/10.1016/j.epsl.2021.116878.

References

Brudzinski, M.R., Thurber, C.H., Hacker, B.R., Engdahl, E.R., 2007. Global prevalence of double Benioff zones. Science 316, 1472–1474. https://doi.org/10.1126/science.1139204.

Class, C., Miller, D.M., Goldstein, S.L., Langmuir, C.H., 2000. Distinguishing melt and fluid subduction components in Umnak Volcanics, Aleutian Arc. Geochem. Geophys. Geosyst. 1. https://doi.org/10.1029/1999gc000010.

Cousens, B., Weis, D., Constantin, M., Scott, S., 2017. Radiogenic isotopes in enriched mid-ocean ridge basalts from Explorer Ridge, northeast Pacific Ocean. Geochim. Cosmochim. Acta 213, 63–90. https://doi.org/10.1016/j.gca.2017.06.032.

Creager, J.S., Scholl, D.W., Boyce, R.E., Echols, R.J., Lee, H.J., Ling, H.Y., Stewart, R.J., Supko, P.R., Worsley, T.R., 1973. Deep sea drilling project initial reports: site 183. DSDP Volume XIX, 1-19.

Davies, J., Sykes, L., House, L., Jacob, K., 1981. Shumagin seismic gap, Alaska Peninsula - history of great earthquakes, tectonic setting, and evidence for high seismic potential. J. Geophys. Res. 86, 3821–3855. https://doi.org/10.1029/JB086iB05p03821.

Ekström, G., Nettles, M., Dziewoński, A.M., 2012. The global CMT project 2004–2010: centroid-moment tensors for 13,017 earthquakes. Phys. Earth Planet. Inter. 200–201, 1–9. https://doi.org/10.1016/j.pepi.2012.04.002.

Faccenda, M., Gerya, T.V., Mancktelow, N.S., Moresi, L., 2012. Fluid flow during slab unbending and dehydration: implications for intermediate-depth seismicity, slab weakening and deep water recycling. Geochem. Geophys. Geosyst. 13, Q01010. https://doi.org/10.1029/2011gc003860.

Florez, M.A., Prieto, G.A., 2019. Controlling factors of seismicity and geometry in double seismic zones. Geophys. Res. Lett. 46, 4174–4181. https://doi.org/10.1029/2018gl081168.

Gavrilenko, M., Krawczynski, M., Ruprecht, P., Li, W., Catalano, J.G., 2019. The quench control of water estimates in convergent margin magmas. Am. Mineral. 104, 936–948. https://doi.org/10.2138/am-2019-6735.

George, R., Turner, S., Hawkesworth, C., Morris, J., Nye, C., Ryan, J., Zheng, S.-H., 2003. Melting processes and fluid and sediment transport rates along the Alaska-Aleutian arc from an integrated U-Th-Ra-Be isotope study. J. Geophys. Res., Solid Earth 108. https://doi.org/10.1029/2002JB001916.

Grove, T.L., Till, C.B., Krawczynski, M.J., 2012. The role of H_2O in subduction zone magmatism. Annu. Rev. Earth Planet. Sci. 40 (40), 413–439. https://doi.org/10.1146/annurev-earth-042711-105310.

Guiraud, M., Powell, R., Rebay, G., 2001. H_2O in metamorphism and unexpected behaviour in the preservation of metamorphic mineral assemblages. J. Metamorph. Geol. 19, 445–454. https://doi.org/10.1046/j.0263-4929.2001.00320.x.

Hacker, B.R., Peacock, S.M., Abers, G.A., Holloway, S.D., 2003. Subduction factory 2. Are intermediate-depth earthquakes in subducting slabs linked to metamorphic dehydration reactions? J. Geophys. Res., Solid Earth 108, 2030. https://doi.org/10.1029/2001jb001129.

Hawkesworth, C.J., Turner, S.P., McDermott, F., Peate, D.W., van Calsteren, P., 1997. U-Th isotopes in Arc magmas: implications for element transfer from the subducted crust. Science 276, 551–555. https://doi.org/10.1126/science.276.5312.551.

Hayes, G.P., Moore, G.L., Portner, D.E., Hearne, M., Flamme, H., Furtney, M., Smoczyk, G.M., 2018. Slab2, a comprehensive subduction zone geometry model. Science 362, 58–61. https://doi.org/10.1126/science.aat4723.

Hegner, E., Tatsumoto, M., 1987. Pb, Sr, and Nd isotopes in basalts and sulfides from the Juan de Fuca Ridge. J. Geophys. Res., Solid Earth 92, 11380–11386. https://doi.org/10.1029/JB092iB11p11380.

Hermann, J., Rubatto, D., 2009. Accessory phase control on the trace element signature of sediment melts in subduction zones. Chem. Geol. 265, 512–526. https://doi.org/10.1016/j.chemgeo.2009.05.018.

Hildreth, W., Moorbath, S., 1988. Crustal contributions to arc magmatism in the Andes of Central Chile. Contrib. Mineral. Petrol. 98, 455–489. https://doi.org/10.1007/BF00372365.

House, L.S., Jacob, K.H., 1983. Earthquakes, plate subduction, and stress reversals in the Eastern Aleutian Arc. J. Geophys. Res. 88, 9347–9373. https://doi.org/10.1029/JB088iB11p09347.

Hudnut, K.W., Taber, J.J., 1987. Transition from double to single Wadati-Benioff seismic zone in the Shumagin Islands, Alaska. Geophys. Res. Lett. 14, 143–146. https://doi.org/10.1029/GL014i002p00143.

Igarashi, T., Matsuzawa, T., Umino, N., Hasegawa, A., 2001. Spatial distribution of focal mechanisms for interplate and intraplate earthquakes associated with the subducting Pacific plate beneath the northeastern Japan arc: a triple-planed deep seismic zone. J. Geophys. Res., Solid Earth 106, 2177–2191. https://doi.org/10.1029/2000jb900386.

Jenner, F.E., O'Neill, H.S.C., 2012. Analysis of 60 elements in 616 ocean floor basaltic glasses. Geochem. Geophys. Geosyst. 13. https://doi.org/10.1029/2011gc004009.

Kelemen, P.B., Yogodzinski, G.M., Scholl, D.W., 2003. Along-strike variation in the Aleutian Island Arc: genesis of high Mg# andesite and implications for continental crust. In: Eiler, J. (Ed.), Inside the Subduction Factory. American Geophysical Union, Washington, DC, pp. 223–276.

Kirby, S., Engdahl, R.E., Denlinger, R., 1996. Intermediate-Depth Intraslab Earthquakes and Arc Volcanism as Physical Expressions of Crustal and Uppermost Mantle Metamorphism in Subducting Slabs, Subduction Top to Bottom. American Geophysical Union, pp. 195–214.

Kirby, S., Kelemen, P., 2019. S11A-07: seismogenesis in the lower zone of double seismic zones by shear instabilities in carbonate domains in subducting oceanic lithosphere. In: 2019 AGU Fall Meeting. San Francisco.

Kita, S., Ferrand, T.P., 2018. Physical mechanisms of oceanic mantle earthquakes: comparison of natural and experimental events. Sci. Rep. 8, 17049. https://doi.org/10.1038/s41598-018-35290-x.

Larsen, J.F., 2016. Unraveling the diversity in arc volcanic eruption styles: examples from the Aleutian volcanic arc, Alaska. J. Volcanol. Geotherm. Res. 327, 643–668. https://doi.org/10.1016/j.jvolgeores.2016.09.008.

Li, S.S., Freymueller, J.T., 2018. Spatial variation of slip behavior beneath the Alaska Peninsula along Alaska-Aleutian subduction zone. Geophys. Res. Lett. 45, 3453–3460. https://doi.org/10.1002/2017gl076761.

Maus, S., Barckhausen, U., Berkenbosch, H., Bournas, N., Brozena, J., Childers, V., Dostaler, F., Fairhead, J.D., Finn, C., von Frese, R.R.B., Gaina, C., Golynsky, S., Kucks, R., Luhr, H., Milligan, P., Mogren, S., Muller, R.D., Olesen, O., Pilkington, M., Saltus, R., Schreckenberger, B., Thebault, E., Tontini, F.C., 2009. EMAG2: a 2-arc min resolution Earth Magnetic Anomaly Grid compiled from satellite, airborne, and marine magnetic measurements. Geochem. Geophys. Geosyst. 10. https://doi.org/10.1029/2009gc002471.

Miller, D.M., Goldstein, S.L., Langmuir, C.H., 1994. Cerium/lead and lead isotope ratios in arc magmas and the enrichment of lead in the continents. Nature 368, 514–520. https://doi.org/10.1038/368514a0.

Nakajima, J., Tsuji, Y., Hasegawa, A., Kita, S., Okada, T., Matsuzawa, T., 2009. Tomographic imaging of hydrated crust and mantle in the subducting Pacific slab beneath Hokkaido, Japan: evidence for dehydration embrittlement as a cause of intraslab earthquakes. Gondwana Res. 16, 470–481. https://doi.org/10.1016/j.gr.2008.12.010.

Pesicek, J.D., Thurber, C.H., Zhang, H., DeShon, H.R., Engdahl, E.R., Widiyantoro, S., 2010. Teleseismic double-difference relocation of earthquakes along the Sumatra-Andaman subduction zone using a 3-D model. J. Geophys. Res., Solid Earth 115. https://doi.org/10.1029/2010jb007443.

Peucker-Ehrenbrink, B., Hofmann, A.W., Hart, S.R., 1994. Hydrothermal lead transfer from mantle to continental crust: the role of metalliferous sediments. Earth Planet. Sci. Lett. 125, 129–142. https://doi.org/10.1016/0012-821X(94)90211-9.

Plank, T., 2005. Constraints from thorium/lanthanum on sediment recycling at subduction zones and the evolution of the continents. J. Petrol. 46, 921–944. https://doi.org/10.1093/petrology/egi005.

Plank, T., 2014. The chemical composition of subducting sediments. In: Keeling, R.F. (Ed.), Treatise on Geochemistry. Elsevier, Amsterdam, pp. 607–629.

Plank, T., Kelley, K.A., Zimmer, M.M., Hauri, E.H., Wallace, P.J., 2013. Why do mafic arc magmas contain ~4 wt% water on average? Earth Planet. Sci. Lett. 364, 168–179. https://doi.org/10.1016/j.epsl.2012.11.044.

Plank, T., Langmuir, C.H., 1998. The chemical composition of subducting sediment and its consequences for the crust and mantle. Chem. Geol. 145, 325–394. https://doi.org/10.1016/S0009-2541(97)00150-2.

Reyners, M., Coles, K.S., 1982. Fine structure of the dipping seismic zone and subduction mechanics in the Shumagin Islands, Alaska. J. Geophys. Res., Solid Earth 87, 356–366. https://doi.org/10.1029/JB087iB01p00356.

Ruff, L.J., 1989. Do trench sediments affect great earthquake occurrence in subduction zones? In: Ruff, L.J., Kanamori, H. (Eds.), Subduction Zones Part II. Birkhäuser, Basel, pp. 263–282.

Ruppert, N.A., 2008. Stress map for Alaska from earthquake focal mechanisms. In: Freymueller, J.T., Haeussler, P.J., Wesson, R.L., Ekström, G. (Eds.), Active Tectonics and Seismic Potential of Alaska. American Geophysical Union, Washington DC.

Scambelluri, M., Cannaò, E., Gilio, M., 2019. The water and fluid-mobile element cycles during serpentinite subduction. A review. Eur. J. Mineral. 31, 405–428. https://doi.org/10.1127/ejm/2019/0031-2842.

Scholz, C.H., 1968. The frequency-magnitude relation of microfracturing in rock and its relation to earthquakes. Bull. Seismol. Soc. Am. 58, 399–415.

Shillington, D.J., Becel, A., Nedimovic, M.R., Kuehn, H., Webb, S.C., Abers, G.A., Keranen, K.M., Li, J.Y., Delescluse, M., Mattei-Salicrup, G.A., 2015. Link between plate fabric, hydration and subduction zone seismicity in Alaska. Nat. Geosci. 8, 961–U998. https://doi.org/10.1038/Ngeo2586.

Singer, B.S., Jicha, B.R., Leeman, W.P., Rogers, N.W., Thirlwall, M.F., Ryan, J., Nicolaysen, K.E., 2007. Along-strike trace element and isotopic variation in Aleutian Island arc basalt: subduction melts sediments and dehydrates serpentine. J. Geophys. Res., Solid Earth 112. https://doi.org/10.1029/2006jb004897.

Stevenson, A.J., Scholl, D.W., Vallier, T.L., 1983. Tectonic and geologic implications of the Zodiac fan, Aleutian Abyssal Plain, northeast pacific. Geol. Soc. Am. Bull. 94, 259–273. https://doi.org/10.1130/0016-7606(1983)94<259:Tagiot>2.0.Co;2.

Sun, S.-s., McDonough, W.F., 1989. Chemical and isotopic systematics of oceanic basalts: implications for mantle composition and processes. Geol. Soc. (Lond.) Spec. Publ. 42, 313–345. https://doi.org/10.1144/gsl.Sp.1989.042.01.19.

van Keken, P.E., Hacker, B.R., Syracuse, E.M., Abers, G.A., 2011. Subduction factory: 4. Depth-dependent flux of H_2O from subducting slabs worldwide. J. Geophys. Res. 116, B01401. https://doi.org/10.1029/2010jb007922.

von Huene, R., Miller, J.J., Weinrebe, W., 2012. Subducting plate geology in three great earthquake ruptures of the western Alaska margin, Kodiak to Unimak. Geosphere 8, 628–644. https://doi.org/10.1130/ges00715.1.

Wang, K.L., 2002. Unbending combined with dehydration embrittlement as a cause for double and triple seismic zones. Geophys. Res. Lett. 29, 1889. https://doi.org/10.1029/2002gl015441.

Wei, S.S., Wiens, D.A., van Keken, P.E., Cai, C., 2017. Slab temperature controls on the Tonga double seismic zone and slab mantle dehydration. Sci. Adv. 3, e1601755. https://doi.org/10.1126/sciadv.1601755.

Wiemer, S., Benoit, J.P., 1996. Mapping the *b*-value anomaly at 100 km depth in the Alaska and New Zealand subduction zones. Geophys. Res. Lett. 23, 1557–1560. https://doi.org/10.1029/96gl01233.

Winslow, H., Ruprecht, P., Stelten, M., Amigo, A., 2020. Evidence for primitive magma storage and eruption following prolonged equilibration in thickened crust. Bull. Volcanol. 82, 69. https://doi.org/10.1007/s00445-020-01406-3.

Wyss, M., Hasegawa, A., Nakajima, J., 2001. Source and path of magma for volcanoes in the subduction zone of northeastern Japan. Geophys. Res. Lett. 28, 1819–1822. https://doi.org/10.1029/2000gl012558.

Yamasaki, T., Seno, T., 2003. Double seismic zone and dehydration embrittlement of the subducting slab. J. Geophys. Res., Solid Earth 108, 2212. https://doi.org/10.1029/2002jb001918.

Yogodzinski, G.M., Brown, S.T., Kelemen, P.B., Vervoort, J.D., Portnyagin, M., Sims, K.W.W., Hoernle, K., Jicha, B.R., Werner, R., 2015. The role of subducted basalt in the source of Island Arc magmas: evidence from seafloor lavas of the Western Aleutians. J. Petrol. 56, 441–492. https://doi.org/10.1093/petrology/egv006.

Zhan, Z., 2017. Gutenberg-Richter law for deep earthquakes revisited: a dual-mechanism hypothesis. Earth Planet. Sci. Lett. 461, 1–7. https://doi.org/10.1016/j.epsl.2016.12.030.

Zhang, H.J., Thurber, C.H., Shelly, D., Ide, S., Beroza, G.C., Hasegawa, A., 2004. High-resolution subducting-slab structure beneath northern Honshu, Japan, revealed by double-difference tomography. Geology 32, 361–364. https://doi.org/10.1130/G20261.2.